Analysis and Design of a Secondary-Side Controlled Active Rectifier for Wireless Battery Charging Application

Fahri Gürbüz[1], Tolga Sürgevil[1], Mutlu Boztepe[2]

[1]Department of Electrical and Electronics Engineering, Dokuz Eylül University, Izmir, Turkey
fahrigurbuz9@hotmail.com, tolga.surgevil@deu.edu.tr
[2]Department of Electrical and Electronics Engineering, Ege University, Izmir, Turkey
mutlu.boztepe@ege.edu.tr

Abstract

In this paper, analysis and design of a current controlled active rectifier on the secondary side of an inductive power transfer (IPT) system is presented. The secondary side controlled rectifier is designed to adjust the battery dc charge current by varying the effective load resistance seen at the secondary coil terminals. Steady-state performance of the IPT system is evaluated based on fundamental harmonic analysis. The current control and gate signal generation schemes of the whole system are built in a simulation model. Theoretical and simulation results of investigated control scheme are shown. Finally, the theoretical results are validated by experimental results obtained from the implemented laboratory prototype.

1. Introduction

Wireless power transfer (WPT) systems have widespread application opportunities at various power levels ranging from a few watts to a few hundreds of kilowatts [1]. In high power applications such as battery charging of electric vehicles, the system efficiency should be high while transmitting power to the vehicle's battery pack. Because of this reason, inductive power transfer (IPT) method is adopted in such systems with two resonated coils operating at a frequency usually lower than 100 kHz [2]. These IPT systems need proper control so as to attain a stabilized charging condition at high efficiency, since the parameter and load variations cause the system to deviate from its designed optimal efficiency point [3-5].

The control of the system can be performed on the primary or secondary side individually or on both [2]. Methods proposed for IPT secondary side current control are used for impedance matching by adjusting the effective resistance at the secondary terminals to maximize efficiency. In order to accomplish this, authors in [5] proposed a buck converter cascaded to the diode rectifier and varied the secondary side load resistance with respect to duty ratio. Authors in [6] proposed a buck and boost converter cascaded to the diode rectifier to keep load resistance constant.

Another approach for secondary side impedance control is the phase-shift method using semi-bridgeless or full-bridge active rectifier topologies proposed in [7-8-9]. In this method, the resistive and reactive parts of the secondary side impedance are varied together depending on the phase-shift angle of the secondary terminal voltage with respect to primary voltage. In order to overcome the limitations of this method, authors in [10-11] proposed a combined control on the duty-cycle and phase-shift angle, which is between the secondary current and fundamental terminal voltage, for separately adjusting the secondary load resistance and reactance by means of a full-bridge active rectifier topology. Recently, the full-bridge active rectifier topology using an additional measurement coil was proposed in [12] for a decoupled control of load impedance to achieve maximum efficiency point tracking.

In this paper, a secondary side current controller is presented for an IPT system. For this purpose, the semi-bridgeless active rectifier topology described in [7-8] is used on the secondary side. While regulating the dc bus current, synchronous rectification proposed in [10-11] is aimed. The performance of this method is compared to pure phase-shift control. The system is analyzed under steady-state conditions using fundamental harmonic approach and by means of simulation models. The theoretical results are verified by the experimental results. This paper is organized as follows: Section-2 describes the steady-state analysis of the IPT system. Section-3 describes operating modes of secondary side controlled rectifier. Section-4 describes the control and pulse generation methods. Section-5 includes simulation and experimental results. Finally, conclusion is drawn in Section-6.

2. Steady-State Analysis

The circuit scheme of the series-series compensated IPT system with a full-bridge inverter on the primary side and a controlled rectifier on the secondary side is shown in Fig.1. In order to analyze the system under steady-state conditions, fundamental harmonic analysis method is used. The equivalent circuit model shown in Fig.2 consists of an air cored transformer circuit with two series resonating capacitors on both sides and load [3]. The battery on the secondary side is considered as an equivalent dc load resistance. It is assumed that V_1 is fundamental sinusoidal voltage source that has an angular frequency of $\omega = 2\pi f_o$, where f_o is the switching frequency of the primary side inverter. L_1, and L_2, are the primary and secondary side self inductances and M is the mutual inductance between the primary and secondary side coils. R_1, R_2, and R_L are parasitic resistor of primary and secondary coil and effective load resistor seen at the secondary terminals, respectively. C_1 and C_2 are the series resonance capacitors on their respective sides. The voltage equations for both sides are written as

$$V_1 = I_1 Z_1 - j\omega M I_2 \quad (1)$$

$$j\omega M I_1 = I_2 Z_2 \quad (2)$$

where $Z_1 = R_1 + j\omega L_1 + 1/j\omega C_1$ is the primary side series impedance and $Z_2 = R_2 + j\omega L_2 + 1/j\omega C_2 + R_L$ is the

secondary side total impedance. From (1) and (2), the primary and secondary side current expressions can be obtained as follows [3]:

$$I_1 = \frac{Z_2}{Z_1 Z_2 + \omega^2 M^2} V_1 \quad (3)$$

$$I_2 = \frac{j\omega M}{Z_1 Z_2 + \omega^2 M^2} V_1 \quad (4)$$

The voltage gain (M_v) and current gain (M_i) of the IPT system are determined as follow [4, 13]:

$$M_v = \left|\frac{V_2}{V_1}\right| = \frac{\omega M R_L}{Z_1 Z_2 + Z_1 R_L + \omega^2 M^2} \quad (5)$$

$$M_i = \left|\frac{I_2}{I_1}\right| = \frac{\omega M}{Z_2} \quad (6)$$

It must be noted that $Z_1 = R_1$ and $Z_2 = R_2 + R_L$ when the system is operating at resonant frequency. Hence, the efficiency of the system under resonance conditions can be obtained as [3, 5]:

$$\eta = \frac{\omega^2 M^2 R_L}{(R_2 + R_L)^2 R_1 + \omega^2 M^2 (R_2 + R_L)} \quad (7)$$

As shown in equations (5)-(7), the voltage and current gains and efficiency depends on the load resistance. When R_L increases, M_i decreases and M_v increases. Maximum efficiency occurs when $M_v = M_i$ as illustrated in Fig.3. This condition can be obtained by matching the load resistance value closely to the mutual reactance value, i.e. $R_L \approx \omega M$ assuming identical coils, as mentioned in [4, 13].

Fig.4 illustrates voltage and current gains and efficiency of the system as a function of operating frequency. It can be seen that maximum efficiency point is slightly above the resonance frequency. System analyses are performed by the coil parameters given in [14] and other system parameters are summarized in TABLE I.

3. Analysis of the Secondary-Side Controlled Active Rectifier

The topology of secondary side controlled active rectifier circuit shown in Fig.1 consists of two upper side diodes D_1, D_2 and two lower side switches S_3, S_4 with anti-parallel diodes D_3, D_4. The conduction angle (β) of the upper side diodes is controlled by the gate pulses of the lower side switches. Hence, the circuit has four operating modes, which are illustrated in Fig.5, depending on the switching states [7-8].

In mode 1 and mode 3, energy transfer to the battery is interrupted via shorting the secondary terminals by turning on the lower side switches (S_3-D_4 in positive half-cycle and S_4-D_3 in negative half-cycle). In mode 2 and mode 4, the secondary side current is commutated to the dc bus through the diode pairs (D_1-D_4 in positive half-cycle and D_2-D_3 in negative half-cycle) by turning off the lower side switches. The power flow to the dc bus can be controlled by properly adjusting the switching durations of S_3-S_4, hence controlling the conduction angle β of upper side diodes, D_1-D_2.

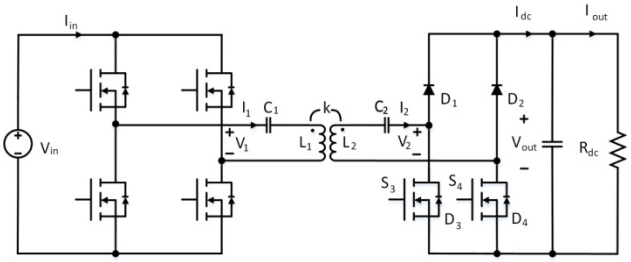

Fig. 1: The IPT system configuration

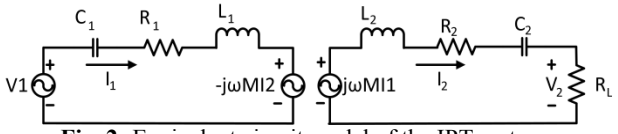

Fig. 2: Equivalent circuit model of the IPT system

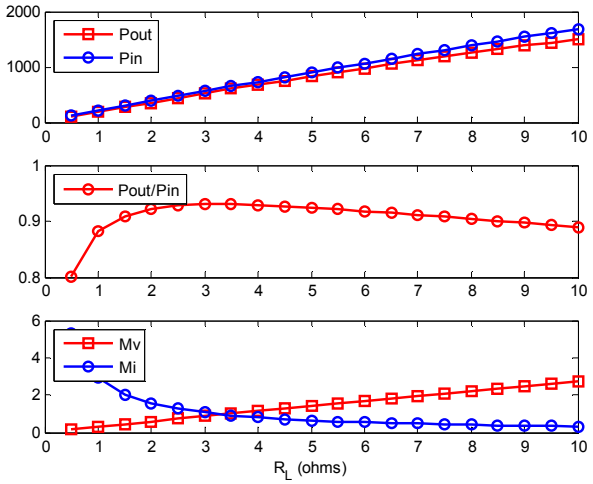

Fig. 3: Variation of (a) input and output power, (b) efficiency, and (c) current and voltage gain with respect to load resistance (V_{in}=50V, f_o=20kHz)

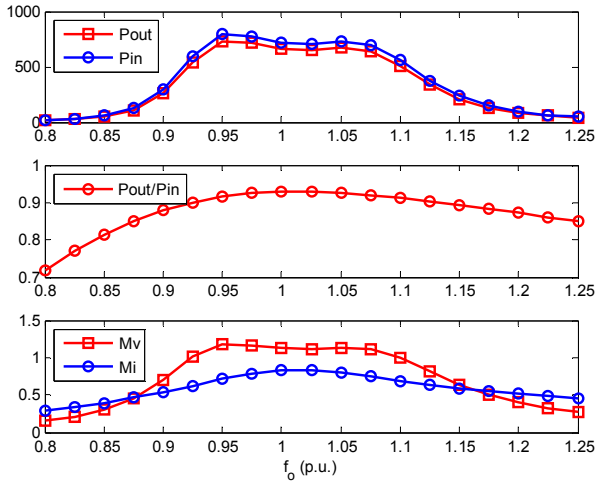

Fig. 4: Variation of (a) input and output power, (b) efficiency, and (c) current and voltage gain with respect to operating frequency (V_{in}=50V, R_L=3.89Ω)

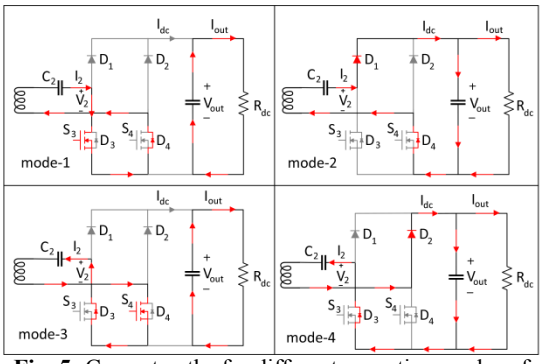

Fig. 5: Current paths for different operating modes of secondary-side rectifier the circuit

The circuit can be controlled in purely resistive (synchronous rectification) or phase-shift (capacitive/inductive) modes to adjust the effective impedance across the circuit input terminals. Fig. 6 illustrates the secondary side voltage and current waveforms for these modes. Purely resistive mode is obtained if conduction angle β is placed symmetrically between two zero crossings of the secondary side current. At this mode, fundamental component of voltage and current is in same phase. This mode is illustrated in Fig. 6(a). Capacitive mode is obtained if conduction angle is aligned to end of the half-cycle where the secondary side current changes polarity from positive to negative. At this mode, fundamental component of secondary terminal voltage lags the current as shown in Fig. 6(b). Inductive mode is obtained if conduction angle is aligned to the beginning of the half-cycle where the zero crossing of the secondary current is from negative to positive. At this mode, current lags the fundamental component of the secondary terminal voltage as shown in Fig. 6(c).

In order to formulate the load characteristic of the controlled rectifier, voltage and current parameters are expressed in terms of dc bus voltage, current, and conduction angle. I_2 is chosen as reference in the calculations. For purely resistive load condition, the secondary voltage and current are in phase. Therefore, the ratio of fundamental peak value of V_2 to I_2 illustrates the load characteristic as shown below:

$$V_2 = \frac{4V_{dc}}{\pi} sin\left(\frac{\beta}{2}\right) \tag{8}$$

$$I_2 = \frac{(\pi/2)I_{dc}}{sin(\beta/2)} \tag{9}$$

$$R_{eq} = \frac{V_2}{I_2} = \frac{8}{\pi^2}(sin\frac{\beta}{2})^2 R_{dc} \tag{10}$$

For reactive load conditions, the load expression is given as follows [7-8];

$$Z_{eq} = \frac{4}{\pi^2} R_{dc}(1 - cos\,\beta)\, sin\left(\frac{\beta}{2}\right) e^{j\left(\frac{\pi}{2}-\frac{\beta}{2}\right)} \tag{11}$$

where $0 \le \beta \le \pi$ for inductive load and $-\pi \le \beta \le 0$ for capacitive load.

Fig. 7 shows the effect of purely resistive and pure phase-shift controls on the efficiency and output power of the IPT system operated under resonance conditions. As shown in Fig.7, the system efficiency remains high for a wide range of conduction angle. However, maximum efficiency of purely resistive control is higher when it is compared to pure phase shift control.

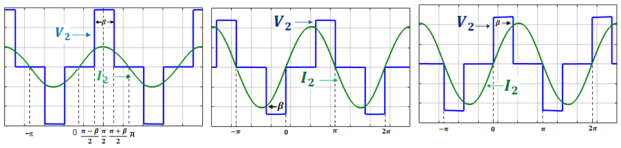

Fig. 6: Secondary voltage and current waveforms for (a) resistive, (b) capacitive, and (c) inductive loading conditions

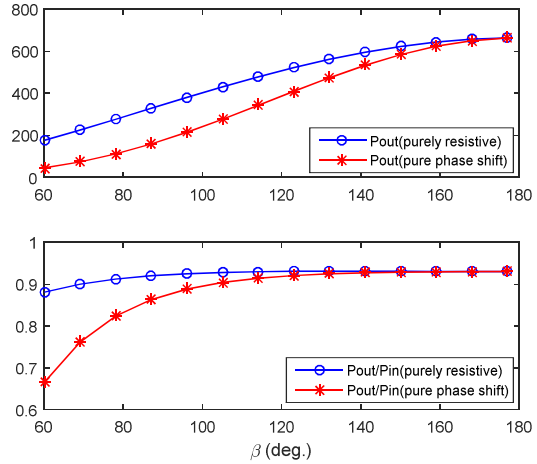

Fig. 7: Comparison of the effects of purely resistive control and pure phase shift control on the output power and efficiency of the IPT system

4. Control Strategy

The current controller block diagram is shown in Fig. 8. To simplify the analysis, the battery is modeled by an equivalent resistor. Hence, as mentioned in the previous section, the secondary side rectifier is controlled to adjust the effective resistance value across the secondary terminals.

The current controller senses the battery current and its value is compared to a reference value. The error between the reference and actual values of the battery current is evaluated by a PI controller. The PI controller calculates the β value. In order to obtain resistive mode operation, the gate pulses must be applied to the switches from the zero crossings of the secondary current symmetrically. By means of a counter, a sawtooth waveform is generated on each half-cycle by resetting the counter at each zero-crossing of the secondary current. The gate pulses are generated by comparing the sawtooth waveform by two comparison values obtained from the PI controller output. Fig. 8 and Fig. 9 show the detailed block diagram of gate pulse generation and waveforms.

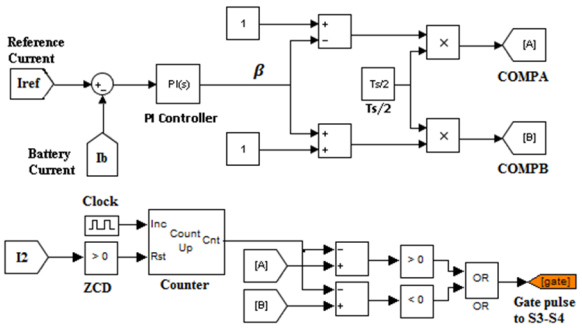

Fig. 8: Current control block diagram

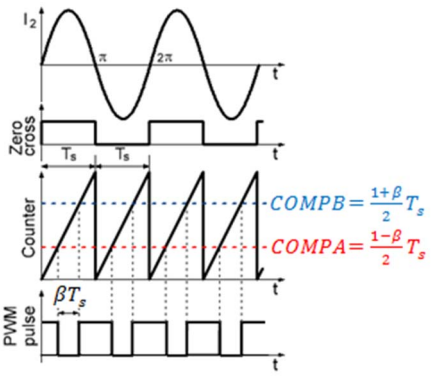

Fig. 9: The gate pulse generation of secondary-side rectifier

5. Simulation and Experimental Results

The secondary side active rectifier is designed to be controlled in resistive mode. The measured system parameters are given in TABLE I. The system is fed from an adjustable buck converter controlled dc voltage source. The power is delivered to a resistor load connected to the secondary side rectifier output. Although the designed coil distance is 150 mm in [14], it is reduced to 75mm in order to increase the coupling coefficient, since it greatly reduces the primary current magnitude. Control software was developed on TMS320F28027 LaunchPad™ microcontroller board. Discrete power IGBTs are used in the controlled rectifier. Both IGBTs are triggered by the same PWM gate signal, which is generated by the controller.

Fig. 10 shows the simulation results, while Fig.11 shows experimental results for comparison purpose and they are observed to be in agreement. The experiments are performed at an operating frequency 5 percent higher than resonant frequency so as to achieve higher coil efficiency. At transmitter side, 1 µs dead time is applied between primary side inverter switches of the same leg. In Fig.12, the variation of the dc load current is shown when the secondary-side dc current reference (I_{ref}) is changed between 2A and 4A. The current PI controller successfully controls the required dc load current. The input and output dc quantities and corresponding efficiency values of the IPT system measured on experimental setup are given in TABLE II.

TABLE I. SYSTEM PARAMETERS

Parameter	***Description***	***Value***
k	Coupling coefficient	0.45
f_o	Operating frequency	20.6 kHz
L_1, L_2	Self inductance of IPT coils	140 µH
C_1, C_2	Resonant capacitor	470nF
R_1, R_2	Coil resistors	0.2 Ω
Rdc	DC Load resistor	16 Ω
C_{dc}	Secondary side dc bus capacitor	470 µF

TABLE II. MEASURED RESULTS

$V_{in}(V)$	$I_{in}(A)$	$V_{out}(V)$	$I_{out}(A)$	η (%)
60	2	33.6	2	56
60	5.8	66.5	4	76.4
70	10.9	98.5	6	77.5

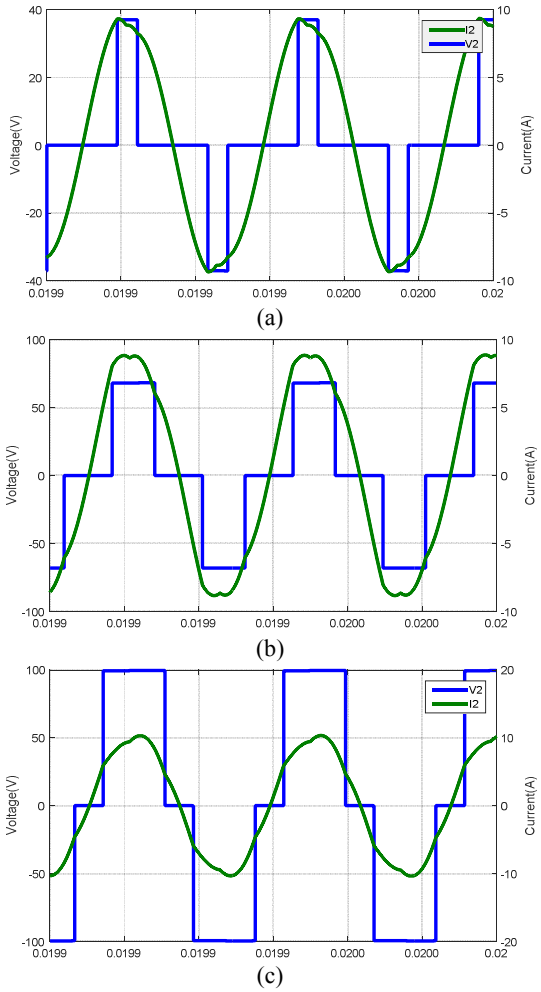

Fig. 10: Simulation results of the secondary voltage and current when (a) V_{in}=60V and I_{ref}=2A, (b) V_{in} =60V and I_{ref} =4A, and (c) V_{in} =70V and I_{ref} =6A

6. Conclusion

In this study, a secondary side controlled rectifier in an IPT system for battery charging of EVs is designed and examined in details. The steady-state analyses of the designed IPT system were presented. Also, the operating modes of the secondary side rectifier are discussed. Impedance equations for resistive, capacitive and inductive mode are formulated and waveforms of different working modes are illustrated. The designed controller to adjust the battery charge current was implemented and tested in the laboratory. The experimental results obtained from the laboratory are in agreement with theoretical results. The overall system efficiency values depend on output power level and determined by the coil and converter losses, which will be analyzed in detail as a future work.

Acknowledgment

This study has been carried out as a part of the project "Design and Optimization of a Contactless Charging System for Electric Vehicles" supported by "The Scientific and Technological Research Council of Turkey (TÜBİTAK)" under project grant number 115E116.

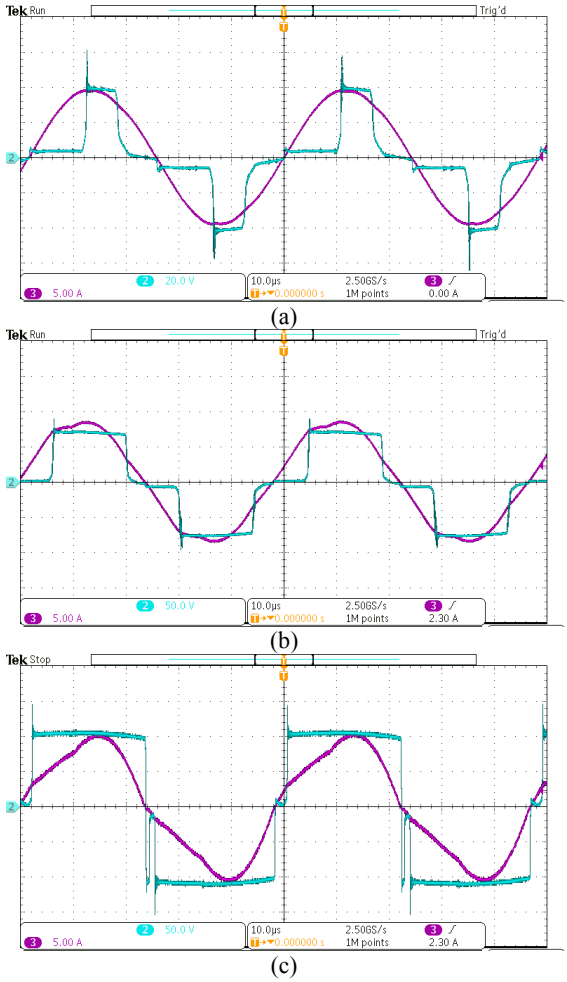

Fig. 11: Experimental results of secondary voltage and current when (a) V_{in} =60V and I_{ref} =2A, (b) V_{in} =60V and I_{ref} =4A, and (c) V_{in} =70V and I_{ref} =6A

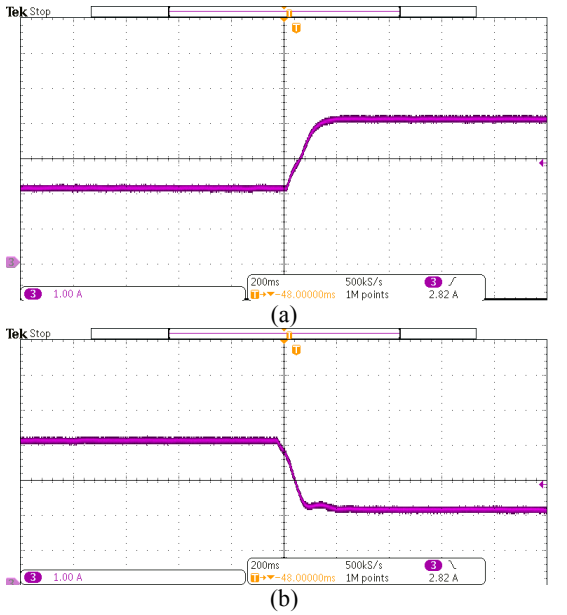

Fig. 12: Experimental results showing the variation of the secondary load current when the reference current is set (a) from 2A to 4A (b) from 4A to 2A

7. References

[1] M.P. Kazmierkowski and A.J. Moradewicz, "Unplugged but connected: Review of Contactless Energy Transfer Systems," IEEE Industrial Electronics Magazine, vol.6, issue 4, pp. 47-55, Dec. 2012.

[2] S. Li and C.C. Mi, "Wireless power transfer for electric vehicle applications," IEEE Journal of Emerging and Selected Topics in Power Electronic, vol. 3, no.1, pp. 4-17, Mar. 2015.

[3] M. Bertoluzzo, R.K. Jha, and G. Buja "Series-series resonant IPT system analysis under frequency mismatch", in 41st Annual Conference of IEEE Industrial Electronics Society (IECON), Yokohama, Japan, Nov. 2015, pp. 439-444.

[4] M. Bojarski, E. Asa, and D. Czarkowski, "Effect of Wireless Power Link Load Resistance on the Efficiency of the Energy Transfer", in IEEE International Electric Vehicle Conference (IEVC), Florence, Italy, Dec. 2014, pp.1-7.

[5] M. Kato, T. Imura, and Y. Hori "Study on maximize efficiency by secondary side control using DC-DC converter in wireless power transfer via magnetic resonant coupling," in World Electric Vehicle Symposium and Exhibition (EVS27), Barcelona, Spain, Nov. 2013, pp. 1-5.

[6] K. Colak, M. Bojarski, E. Asa, and D. Czarkowski "A constant resistance analysis and control of cascaded buck and boost converter for wireless EV chargers," in IEEE Applied Power Electronic Conference and Exposition (APEC), Charlotte, NC, USA, Mar. 2015, pp. 3157-3161.

[7] K. Colak, M. Bojarski, E. Asa, D. Czarkowski , and O.C. Omar, "A novel phase shift control of semibridgeless active rectifier for wireless power transfer," IEEE Transactions on Power Electronics, vol. 30, no. 11, pp. 6288-6297, Nov. 2015.

[8] E. Asa, K. Colak, M. Bojarski, and D. Czarkowski, "A Novel Phase Control of Semi Bridgeless Active Rectifier for Wireless Power Transfer Applications", in IEEE Applied Power Electronics Conference and Exposition (APEC), Charlotte, NC, USA, Mar. 2015, pp. 3225-3231.

[9] C. Zhao, Z. Wang, J. Du, J. Wu, S. Zong, and X. He, "Active resonance wireless power transfer system using phase shift control strategy," in IEEE Applied Power Electronic Conference and Exposition (APEC), Fort Worth, TX, USA, Mar.2014, pp. 1336-1341.

[10] A. Berger, M. Agosttinelli, S. Vesti, J.A. Oliver, J.A. Cobos, and M. Huemer, "A wireless charging system applying phase shift and amplutude control to maximize efficiency and extractable power", IEEE Transactions on Power Electronics, vol. 30, no. 11, pp. 6338-6348, Nov. 2015.

[11] A. Berger, M. Agostinelli, S. Vesti, J.A. Oliver, J.A. Cobos, and M. Huemer, "Phase-Shift and Amplitude Control for an Active Rectifier to Maximize the Efficiency and Extracted Power of a Wireless Power Transfer System", in IEEE Applied Power Electronics Conference and Exposition (APEC), Charlotte, NC, USA, Mar. 2015, pp.1620-1624.

[12] R. Mai, Y. Liu, Y. Li, P. Yue, G. Cao, and Z. He, , "An Active Rectifier Based Maximum Efficiency Tracking Method Using an Additional Measurement Coil for Wireless Power Transfer", IEEE Transaction on Power Electronics, Feb. 2017, doi: 10.1109/TPEL.2017.2665040.

[13] R. Bosshard, J.W. Kolar, J. Mühlethaler, I. Stevanovich, B. Wunsch, and F. Canales, "Modelling and α-η-Pareto optimization of inductive power transfer coils for electrical vehicle," IEEE Journal of Emerging and Selected Topics in Power Electronic, vol. 3, no. 1, pp. 50-64, Mar., 2015

[14] Y. Tezcan, H. Ünal, T. Sürgevil, and M. Boztepe, " Optimum Coil Design Considering Skin and Proximity Effects for a Wireless Battery Charger of Electric Vehicle", World Electromobility Conference (WELMO 2017), İzmir, Turkey, May 2017, pp.1-5.